NANO LETTERS

pubs.acs.org/NanoLett

Heat Conduction across Monolayer and Few-Layer Graphenes

Yee Kan Koh,*,†,§ Myung-Ho Bae,‡ David G. Cahill,† and Eric Pop‡

†Department of Materials Science and Engineering and Frederick Seitz Materials Research Laboratory, University of Illinois, Urbana, Illinois 61801, United States, ‡Department of Electrical & Computer Engineering, Micro and Nanotechnology Lab, University of Illinois, Urbana, Illinois 61801, United States, and §Department of Mechanical Engineering, National University of Singapore, Singapore

ABSTRACT We report the thermal conductance G of Au/Ti/graphene/SiO_2 interfaces (graphene layers $1 \le n \le 10$) typical of graphene transistor contacts. We find $G \approx 25$ MW m^{-2} K^{-1} at room temperature, four times smaller than the thermal conductance of a Au/Ti/SiO_2 interface, even when $n = 1$. We attribute this reduction to the thermal resistance of Au/Ti/graphene and graphene/SiO_2 interfaces acting in series. The temperature dependence of G from $50 \le T \le 500$ K also indicates that heat is predominantly carried by phonons through these interfaces. Our findings suggest that metal contacts can limit not only electrical transport but also thermal dissipation from submicrometer graphene devices.

KEYWORDS Interfacial thermal conductance, few-layer graphene, metal contacts, acoustic phonons, heat dissipation, thermal management of graphene devices

Graphene, a monolayer or few layers of sp^2-bonded carbon atoms, has attracted immense attention over the past few years partly due to the prospect of replacing III−V semiconductors as the workhorse of high-frequency electronics.[1] In addition to superior electrical properties (mobility ∼10000 cm^2 V^{-1} s^{-1} at room temperature[2] on SiO_2 at practical carrier concentrations ∼10^{12} cm^{-2}), graphene also has exceptionally high in-plane thermal conductivity[3,4] on the order ∼1000 W m^{-1} K^{-1}, which is advantageous for thermal management. High in-plane thermal conductivity, however, implies that heat dissipation from graphenes is also affected by how heat flows across its interfaces.

In this Letter, we report the thermal conductance G of Au/Ti/graphene/SiO_2 interfaces which are typically found in graphene devices,[5] for number of graphene layers $1 \le n \le 10$ and a temperature range of $50 \le T \le 500$ K. We find $G \approx 25$ MW m^{-2} K^{-1} irrespective of n at room temperature and that heat flow across the metal/graphene/SiO_2 interface is limited by G of the metal/graphene interface rather than the graphene/SiO_2 interface. Thus, the choice of metal contacts affects both electrical[6] and thermal transport[5] in graphene devices.

While in-plane heat transport in graphene can be attributed to acoustic vibrational modes called phonons,[4,7] the dominant heat carriers across graphene interfaces in the cross-plane direction are not known. Even under the absence of an external electric field, graphene could have substantial carrier density[6] on the order of 10^{13} cm^{-2} due to charge transfer from metal contacts.[8] Since the density of free carriers (electrons or holes) is high on both sides of the interface, heat transport across a metal/graphene interface could be facilitated by free carriers instead of phonons, analogous to heat transport by electrons across metal/metal interfaces.[9] Moreover, since carriers in graphene are readily scattered by polar optical phonons (sometimes called remote interfacial phonons or surface-optical phonons) in the SiO_2 substrate,[2,10] heat transport through graphene/SiO_2 interfaces could have a contribution from direct energy transfer[11] between free carriers in graphene and polar optical phonons in SiO_2.

To identify the dominant heat carriers across graphene/metal and graphene/SiO_2 interfaces, we measured the thermal conductance G of Au/Ti/graphene/SiO_2 interfaces over a temperature range of $50 \le T \le 500$ K. We find that G of such interfaces depends only weakly on temperature above 100 K. The temperature dependence of G is expected to follow the temperature dependence of heat capacity for the excitations that are most responsible for heat conduction.[12] The heat capacity of the degenerate electrons in Au and the heat capacity of optical phonons in SiO_2 increase significantly between 100 and 500 K; the contribution of acoustic phonons to the heat capacity of Au, on the other hand, is essentially constant in this temperature range due to the low Debye temperature of Au. Therefore, we conclude that acoustic phonons are the dominant carriers of heat across these interfaces.

Even when an interface is atomically abrupt, heat transport by phonons across it is limited by the finite probability of phonon transmission; the resulting impedance to heat flow is characterized by a property of an individual interface called the Kapitza thermal conductance,[12] G_I. The total thermal conductance per unit area G of a thin film sand-

* Corresponding author. Email: mpekyk@nus.edu.sg.
Received for review: 05/21/2010
Published on Web: 10/05/2010

© 2010 American Chemical Society

DOI: 10.1021/nl101790k | *Nano Lett.* **2010,** *10,* 4363–4368

wiched between two solids can often be attributed to the series sum of contribution from two discrete interfaces and the bulk of the thin film.[13] If this assumption were valid for the case of metal/graphene/SiO_2 interfaces, we could write

$$G^{-1} = (G_I^{-1})_{\text{metal}/n\text{-LG}} + (G_I^{-1})_{n\text{-LG}/SiO_2} + (h/\Lambda)_{n\text{-LG}} \quad (1)$$

where h and Λ are the thickness and the cross-plane thermal conductivity of n-layer graphene (n-LG), respectively, and h/Λ is the corresponding thermal resistance per unit area. Assuming $\Lambda > 1$ W m^{-1} K^{-1}, $h/\Lambda < 10^{-9}$ m^2 K W^{-1} and is negligible compared to G_I^{-1}.

When the film is sufficiently thin, however, phonons (especially long-wavelength phonons) could, in principle, traverse directly between the metal and SiO_2 without being scattered by the interfaces.[14] In such cases, eq 1 is invalid, and we should treat the structure as one diffuse interface instead of two discrete interfaces. Factors dictating at what film thickness eq 1 breaks down are not yet established. However, from our measurements on G of Au/Ti/graphene/SiO_2 interfaces, we find that G remains unchanged for number of graphene layers of $1 \le n \le 10$ (equivalent to thickness of $0.4 \le h \le 4$ nm). Moreover, the measured G is comparable to the G calculated using eq 1 over a temperature range of $50 \le T \le 500$ K. Thus, our results suggest that, even when the graphene layer is only one atomic layer thick, heat transport across the metal/graphene/oxide interfaces is governed by the thermal conductance of two (metal/graphene and graphene/oxide) uncoupled interfaces. This indicates that heat conduction due to direct transmission of phonons between Au and SiO_2 is negligible.

Our test structures resemble typical metal contacts in graphene devices;[5] see Figure 1a. Prior to deposition of graphene, we cleaned selected SiO_2/Si substrates by 10 min of sonication in acetone and/or heat treatment at 200 °C in ambient for 1 h; we noticed no difference in the measured G with or without precleaning. We deposited graphene on 104 nm SiO_2 on Si by micromechanical exfoliation[15] from natural graphite. We then annealed the substrate in a chemical vapor deposition (CVD) furnace at 400 °C for 35 min in Ar/H_2 mixture gas to remove the adhesive residue from the tape. We patterned ≈100 nm thick Au pads on selected graphene flakes by e-beam lithography, e-beam evaporation, and lift-off with ≈2 nm Ti predeposited as the adhesion layer. E-beam evaporation was performed at a base-pressure of 7×10^{-7} Torr, and the Au and Ti were deposited at rates of 2.5 and 0.5 Å/s, respectively. Due to low deposition rate of Ti, a significant amount of oxygen could be trapped in the Ti film. We note that even though the metal films were deposited in vacuum, water vapor that adsorbs on the substrate during the air exposure after the annealing step may still be present during the deposition of the Au/Ti contacts. We purposely deposited large metal pads

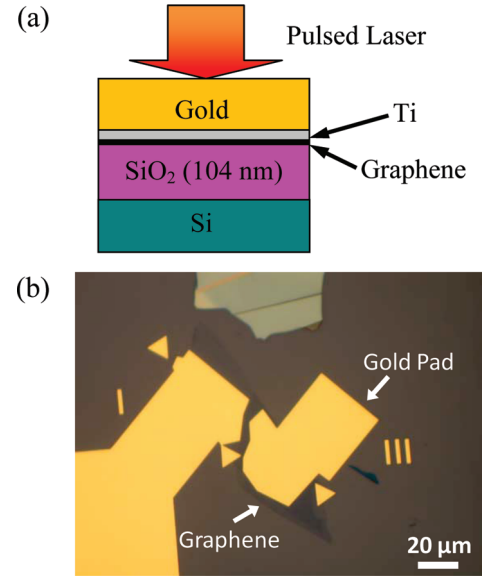

FIGURE 1. (a) Vertical cross section of the samples (not-to-scale). Au(100 nm)/Ti(2 nm) thin metal pads were patterned on graphene flakes on SiO_2 (104 nm) on Si substrate by e-beam lithography. (b) Example optical microscopy image of a graphene sample covered by metal pads.

on our samples such that the same metal pad covers both regions with and without graphene flakes; see Figure 1b. Time-domain thermoreflectance (TDTR) measurements, discussed below, were performed on both regions with and without graphene flakes covered by the same metal pads to derive G of Au/Ti/graphene/SiO_2 interfaces.

Our samples consist of graphenes with number of layers from $1 \le n \le 10$, denoted by n-LG (n layers of graphene) throughout this work. We employed a newly developed approach based on Raman spectroscopy[16] to count the number of layers n of the graphene flakes. In this approach, n is determined from the ratio of the integrated intensity of Raman peak at ∼520 cm^{-1} due to scattering by optical phonons in silicon, I(Si), and integrated intensity of G peak due to scattering by doubly degenerate in-plane optical phonons (iTO and LO) in graphene, I(G); see Figure 2a. We validated n derived using this approach by measuring the thickness of the graphenes by atomic force microscopy (AFM); a more complete description of this approach will be published in ref 16. We measure the Raman spectra of graphenes by a custom-built Raman spectrometer; a 488 nm laser beam excites the Raman spectra. We use laser powers of ≈1 mW in our measurements and a 20× objective lens with N.A. = 0.4 to focus the laser beam and collect Raman-scattered light in all polarizations. The full width half-maximum spectral resolution of our Raman setup is ≈6 cm^{-1}.

To verify that the graphene flakes are not damaged by deposition of Au/Ti, we coated a monolayer graphene (1-LG) sample with a semitransparent layer of Au (8 nm)/Ti (2 nm) and compared the Raman spectrum of the sample before and after metal deposition; see Figure 2b. We observe

© 2010 American Chemical Society

DOI: 10.1021/nl101790k | Nano Lett. 2010, 10, 4363–4368

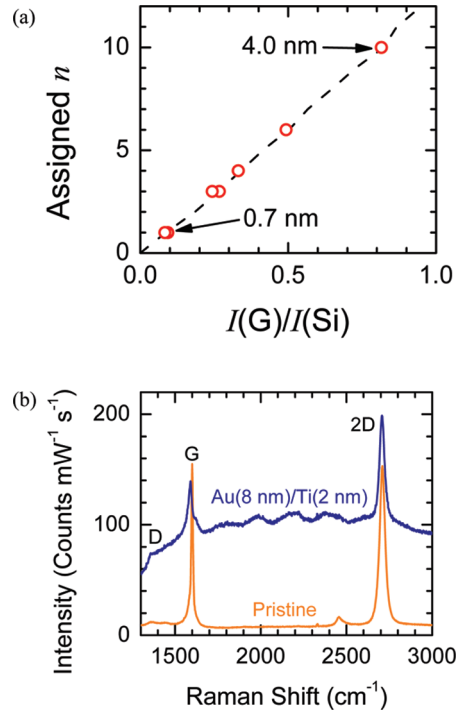

FIGURE 2. (a) Determining graphene layer number (*n*) from ratios of integrated intensity of the Raman peak due to scattering by optical phonons in silicon, *I*(Si), and integrated intensity of graphene G peak, *I*(G). The Raman spectra were acquired using a 488 nm laser. Raman measurements (open circles) are compared to average *I*(G)/*I*(Si) values from ref 16 (dashed line) to determine the number of layers *n*. The thickness of two selected graphene flakes is measured by atomic force microscopy (AFM), as labeled. (b) Raman spectra of monolayer graphene before and after coverage with Au (8 nm)/Ti (2 nm). The spectrum of graphene after metal deposition is vertically down-shifted by 170 counts mW^{-1} s^{-1} for clarity. D peaks (defect-mediated Raman scattering from iTO phonons near the Brillouin zone boundary) are weak in both spectra, indicating that metal deposition does not significantly damage the graphene structure. Metal deposition causes the G peak to split into two slightly broadened peaks centered at 1590 and 1622 cm^{-1}.

a distinct 2D peak (due to two iTO phonons near Brillouin zone boundary) at 2707 cm^{-1} with a fwhm of 35 cm^{-1} after the deposition of thin metal layers. This narrow 2D peak at ~2700 cm^{-1} is a fingerprint[17] of monolayer graphene and indicates that graphene was not significantly damaged by e-beam deposition of the metal film. The D peak (due to one iTO phonon near Brillouin zone boundary and defects) at ~1350 cm^{-1} is weak after the metal deposition, suggesting that the density of graphene defects remains low. The G peak is slightly split and broadened after metal evaporation; see Figure 2b. This change of shape is inconsistent with a sharpened, red-shifted G peak due to Landau damping and stiffening of phonons by high carrier concentrations in graphene;[18] we are unsure of the cause of these changes in the shape of the G peak but interactions between the G-band optical phonons in graphene and the electronic excitations of the metal may be playing a role.

We measure the thermal conductance G by time-domain thermoreflectance[19,20] (TDTR). A schematic diagram of our equipment is given in ref 20 and our method for data analysis is described in ref 21. In our TDTR measurements, a laser beam from a mode-locked Ti:sapphire laser is split into a pump beam and a probe beam with the relative optical path being adjusted via a mechanical delay stage. The pump beam is modulated at a frequency $f = 10$ MHz. Laser pulses of the pump beam of <1 nJ are absorbed by the Au pads, inducing a temperature oscillation of <10 K at the surface of the Au pads. Cooling of the surface after being heated by pump pulses is then monitored through changes in the intensity of the reflected probe beam using a Si photodiode and a lock-in amplifier. The radii of the laser beams used during the measurements are either 7.5 or 3.8 μm at the sample surface. We used total laser powers of <110 mW for laser spot size of 7.5 μm and <45 mW for laser spot size of 3.8 μm, creating temperature rises of <10 K. The ratios of the power of the pump beam to the probe beam vary from 1:1 to 20:1; as expected, we did not observe any difference in the derived G using different power ratios.

To enhance the accuracy of G of Au/Ti/n-LG/SiO_2 interfaces derived using TDTR, we performed TDTR measurements on adjacent regions with and without graphene flakes for every graphene flake we studied. We compared the ratio of in-phase and out-of-phase of the lock-in amplifier of both measurements to numerical solutions of a thermal model[21] that takes into account changing of the radius of the pump beam at different relative delay times;[22] see Figure 3a. We first take $G = 100$ MW m^{-2} K^{-1} for Au/Ti/SiO_2 interfaces (this value of G was prior measured using a 500 nm SiO_2 coated with Au/Ti) and lump the uncertainty of TDTR measurements by deriving the thermal conductivity of SiO_2 thin films from initial measurements on regions without graphene flakes. Since the uncertainty should be similar for measurements on adjacent regions with graphene flakes, we then derived G of Au/Ti/n-LG/SiO_2 interfaces by fitting the second TDTR measurements on regions with graphene flakes using the thermal conductivity of SiO_2 previously derived. The uncertainty of G for Au/Ti/n-LG/SiO_2 interfaces derived using this approach is ≈20%. The main contributor to this is the uncertainty (≈35%) in G of the Au/Ti/SiO_2 interfaces, which contributes ≈12% to the total uncertainty.

We plot G of Au/Ti/n-LG/SiO_2 interfaces as a function of number of graphene layer n in Figure 3b. We find that at room temperature $20 < G < 30$ MW m^{-2} K^{-1} for Au/Ti/n-LG/SiO_2 interfaces, irrespective of n; this value of G is a factor of 4 smaller than $G = 100$ MW m^{-2} K^{-1} directly measured on our control Au/Ti/SiO_2 interfaces; see Figure 3b. Similar values of thermal conductance were reported for Au/SAM/GaAs interfaces,[23] in which a self-assembled monolayer (SAM) of alkanedithiols is sandwiched between Au and GaAs.

We note that this relatively high value of G for Au/Ti/n-LG/SiO_2 interfaces implies that graphene capped with metals cannot be partially suspended between asperities of SiO_2 substrate, which is generally perceived to be the case for uncapped graphenes supported on SiO_2.[24,25] If the capped

© 2010 American Chemical Society

DOI: 10.1021/nl101790k | *Nano Lett.* **2010,** *10,* 4363–4368

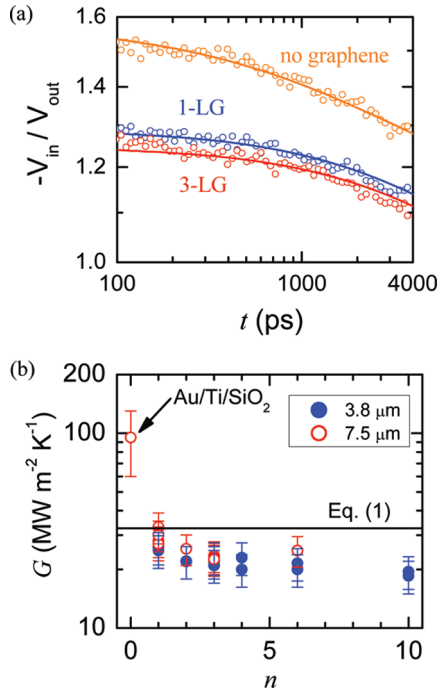

FIGURE 3. (a) Ratios of in-phase and out-of-phase signals (open circles) measured by the lock-in amplifier as a function of delay time t between pump and probe pulses. Measurements on Au/Ti/SiO_2/Si (no graphene), Au/Ti/1-LG/SiO_2/Si, and Au/Ti/3-LG/SiO_2/Si are labeled as "no graphene", "1-LG", and "3-LG", respectively. The monolayer (1-LG) and trilayer (3-LG) graphenes are deposited on the same substrate and covered with metal pads under the same conditions, as shown in Figure 1b. The solid lines are calculations of a thermal model. (b) Thermal conductance G per unit area of Au/Ti/n-LG/SiO_2 measured by TDTR using laser beams with $1/e^2$ spot size of 7.5 μm (open circles) and 3.8 μm (solid circles) as a function of number of layers n; $n = 0$ corresponds to G of the Au/Ti/SiO_2 interface. The solid line is a calculation using eq 1. The uncertainty of measurements is ≈20%.

graphene were suspended between asperities of SiO_2, the contact area between graphene and SiO_2 would be small and the thermal conductance of graphene/SiO_2 interfaces extremely low. For example, if graphenes in our measurements were partially suspended across voids with a contact area of <10%, our measurements indicate that the real thermal conductance of the metal/graphene/oxide is >250 MW m^{-2} K^{-1}, inconsistent with our measurement of G of an Au/Ti/SiO_2 interface and prior measurements of $G \approx 85$ MW m^{-2} K^{-1} for the 1-LG/SiO_2 interfaces[26] and $G < 120$ MW m^{-2} K^{-1} for the metal/graphite interfaces.[27] Thus, our results indicate that either the capped graphene conforms[28] to the SiO_2 substrate or the voids are filled with water or hydrocarbons that can carry heat across the gap.

Our assertion that the encased graphenes conform to the substrate is reinforced by our time-domain pump-beam-deflection[29] (TD-PBD) measurements of the acoustic waves reflected by interfaces with and without graphenes. We find that the shape and amplitude of the acoustic reflections are comparable with and without graphenes. Since voids with zero acoustic impedance should vastly enhance the acoustic reflection, our findings suggest that the area occupied by voids is a small fraction of the total area.

Our values for G of graphene contacts suggest that heat dissipation from graphene field-effect transistors (GFETs) with dimensions $L < 600$ nm will often be affected by the thermal conductance of graphene interfaces. To estimate the importance of graphene interfaces in the thermal management of GFETs supported on SiO_2/Si, we assume that heat is generated at the center of the GFET and can dissipate to the surroundings either through metal contacts or the SiO_2 substrate. The dominant path of heat dissipation is governed by a characteristic length called the thermal healing length[30,31]

$$l_h = \sqrt{h\Lambda/G} \qquad (2)$$

where $h = 0.35$ nm and $\Lambda \approx 1000$ W m^{-1} K^{-1} are the thickness and in-plane thermal conductivity of monolayer graphene and $1/G = 1/G_{1\text{-LG/SiO}_2} + h_{SiO_2}/\Lambda_{SiO_2}$. For monolayer graphene supported on $h_{SiO_2} = 100$ and 300 nm, $l_h \approx 180$ and 290 nm, respectively. For $L < 2l_h$, heat dissipates from the graphene mainly through the metal contacts; while for $L > 2l_h$, heat dissipates mainly through the SiO_2 substrate. Although most current graphene devices have $L > 2l_h$, the characteristic dimensions of future graphene devices will be reduced $<2l_h$ leading to heat dissipation mainly through the metal contacts.

To estimate the importance of G compared to other thermal resistances of a GFET, we consider a hypothetical device of length $L = 100$ nm between contacts, width $W = 400$ nm, on $h_{SiO_2} = 100$ nm, and 100×400 nm^2 metal contact area. The estimated heat flow resistances through one contact, along the graphene, and through the SiO_2 are $R_C \approx 10^6$ K W^{-1}, $R_G \approx 7.1 \times 10^5$ K W^{-1}, and $R_{SiO_2} \approx 2.2 \times 10^6$ K W^{-1}, respectively. While heat dissipation from GFETs will depend on the realistic three-dimensional geometry of the device, this simple estimate reveals the heat flow path through the metal contacts could in fact be significant for thermal management of future graphene devices.

To further enhance our understanding of heat conduction across graphene, we measured G of Au/Ti/n-LG/SiO_2 interfaces over a wide temperature range of $50 \le T \le 500$ K; see Figure 4. As introduced above, the lack of temperature dependence of G for $T > 100$ K as in Figure 4 supports our assertion that the dominant heat carriers across Au/Ti/n-LG and n-LG/SiO_2 interfaces are acoustic phonons and not free carriers[9] or direct coupling[11] of free carriers in graphene and optical phonons in SiO_2. Our conclusion that free carriers are not responsible for heat conduction across graphene interfaces is also consistent with an estimate using the interface form of the Wiedemann–Franz law.[9] For a graphene/metal contact area $A = 100$ μm^2 with an electrical resistance[32] $R_e \approx 10$ Ω, the thermal conductance at room temperature is $G_e \approx LT/(AR_e) \approx 10$ kW m^{-2} K^{-1} (Lorenz number $L = 2.45 \times 10^{-8}$ Ω W K^{-2}), a factor of 1000 lower than the measured lattice thermal conductance of >10 MW m^{-2} K^{-1}. In other words, except for superb electrical contacts that are yet to be discovered, heat transport across metal/graphene is predominantly carried by phonons.

© 2010 American Chemical Society

DOI: 10.1021/nl101790k | *Nano Lett.* **2010,** *10,* 4363–4368

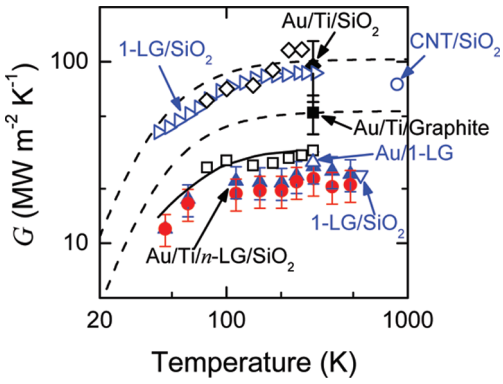

FIGURE 4. Temperature dependence of thermal conductance *G* of Au/Ti/1-LG/SiO_2 (solid triangles) and Au/Ti/3-LG/SiO_2 (solid circles) interfaces. Thermal conductance of Au/Ti/SiO_2 (solid diamond, this work), Au/Ti/graphite (solid square, this work), 1-LG/SiO_2 from Chen et al. (open right triangles, ref 26) and Freitag et al. (open triangle down, ref 11), Au/1-LG (open triange up, Cai et al., ref 37), SWCNT/SiO_2 (open circle, Pop et al., ref 31), Au/graphite (open squares, ref 27), and Ti/graphite (open diamonds, ref 27) are included for comparison. SWCNT denotes single-wall carbon nanotube. The dashed lines are diffuse mismatch model[12] (DMM) calculations for *G* of Au/Ti/SiO_2 (top) and Au/Ti/graphite (bottom) interfaces. The solid line is the prediction of eq 1 using DMM calculations of $G_{Au/Ti/graphite}$ and measurements of $G_{1\text{-}LG/SiO_2}$ from ref 26. Equation 1 agrees with measurements of Au/Ti/*n*-LG/SiO_2 over the entire temperature range.

The reduction of thermal conductance due to the presence of atomic graphitic layers that we observe in Figure 3b could be explained by weaker coupling[33] between metal and oxide. Under this explanation, the metal/graphene/oxide structure is treated as a perturbation that alters the probability for phonons to transmit between metal and oxide, instead of being treated as two discrete interfaces. We argue, however, that this explanation is inadequate especially for thick graphenes of $n = 10$ with layer thickness of ~4 nm. Since most heat is carried by phonons with wavelength <1 nm at room temperature, a 4 nm layer is too thick to be considered a diffuse interface. Moreover, most phonon modes in metal and oxide have relatively low energy (the highest energy of acoustic phonons is 18 and 62 meV in Au and amorphous SiO_2, respectively), but the density of low-energy modes in graphene is small. To give an idea of the density of low-energy modes available in these materials, the ratio of heat capacity of Au, graphite, and SiO_2 at 30 K is 22:1:2.6. Consequently, phonons cannot traverse directly and coherently between metal and oxide.

Instead, we attribute the lower thermal conductance of Au/Ti/*n*-LG/SiO_2 interfaces to Kapitza thermal resistance[12] of Au/Ti/*n*-LG and *n*-LG/SiO_2 interfaces acting in series. To test this hypothesis, we compare our measurements to *G* calculated using eq 1; see the solid line in Figure 3b. In the calculation, we use a prior measurement[26] of *G* of a 1-LG/SiO_2 interface for $G_{1\text{-}LG/SiO_2}$ and approximate $G_{metal/1\text{-}LG}$ from our measurement of *G* of Au/Ti/graphite interfaces. We find that the calculation of eq 1 is in reasonable agreement with our measurements of *G* of Au/Ti/*n*-LG/SiO_2 interfaces. Our finding suggests that even when graphene is only one atomic layer thick, heat is carried across the metal/graphene/oxide interfaces by two-stage transmission of acoustic phonons across metal/graphene and graphene/oxide interfaces.

To further support our assertion that heat transport across the interface is dominated by the Kapitza thermal resistance of two graphene interfaces, we compare our *G* measurements over a wide temperature range to *G* calculated using eq 1 in Figure 4. In the calculations, we use prior measurements[26] of a 1-LG/SiO_2 interface for $G_{1\text{-}LG/SiO_2}$ over the similar temperature range. Since the temperature dependence of *G* of Au/Ti/graphene is not available, we approximate $G_{metal/1\text{-}LG}$ from *G* of Au/Ti/graphite interfaces calculated using the diffuse mismatch model (DMM).[12] Our implementation of the DMM calculations is slightly different from the approach described in ref 12, which is derived for *G* at low temperatures. Following a previous approach to calculations of thermal conductivity[22] at high temperatures, we assume a linear dispersion for phonons in Au and set cutoff frequencies using the frequencies of longitudinal and transverse acoustic phonons at the Brillouin zone boundary in the [100] direction; the cutoff frequencies for longitudinal and transverse phonons in Au are 4.4 and 2.8 THz, respectively. We assume that scattering at the interfaces is elastic and allow mode conversion at the interfaces as long as the energy is conserved. We follow ref 12 and approximate the transmission coefficient α of phonons from Au to SiO_2 using

$$\alpha = \frac{I_{SiO_2}}{I_{SiO_2} + I_{Au}} = \frac{(\Sigma v_j^{-2})_{SiO_2}}{(\Sigma v_j^{-2})_{SiO_2} + (\Sigma v_j^{-2})_{Au}} \qquad (3)$$

where $I_{Au} = (\Sigma v_j^{-2})_{Au}$ is the sum of v_j^{-2} of all phonon modes j available in the Au side and v_j is the speed of sound of phonons with mode j. We note that I_{Au} depends on the phonon frequency ν due to the cutoff frequencies that we impose. For Au to SiO_2, $\alpha = 0.10$ when $\nu < 2.8$ THz and $\alpha = 0.65$ when $\nu > 2.8$ THz. However, the transmission coefficient of phonons from Au to graphite could not be estimated using eq 3 since graphite is highly anisotropic. We therefore derive the effective $I_{graphite} = 6.25 \times 10^{-8}$ s^2 m^{-2} by fitting the calculations to a measurement of $G = 52$ MW m^{-2} K^{-1} for an Au/Ti/graphite interface at room temperature; see Figure 4. The derived α for Au to graphite is then $\alpha = 0.04$ when $\nu < 2.8$ THz and $\alpha = 0.40$ when $\nu > 2.8$ THz. Our approach of deriving α from fitting is compatible to the approach by ref 34, which estimates α from the two-dimensional density of states in graphite.

Our measurements of *G* agree well with the calculations using eq 1 over the entire temperature range, see Figure 4, indicating that heat flow across graphene is governed by the Kapitza thermal conductance of the two interfaces acting in series. Our finding that the bulk of graphene does not significantly contribute to total thermal resistance of graphene in the cross-plane direction is consistent with similar conclu-

© 2010 American Chemical Society

DOI: 10.1021/nl101790k | *Nano Lett.* **2010,** *10,* 4363–4368

sions reached for heat flow across carbon nanotubes,[31,35] SAMs,[23] and molecular chains,[36] which are also limited by interfaces and thus are insensitive to the size of the nanotubes, SAMs, or the molecular chains. Similar results are observed in graphene; see Figure 3b.

In conclusion, we find that heat conduction across metal/graphene/oxide interfaces is limited by finite transmission of phonons between metal and graphene. Thus, for thermal management of graphene devices, metals with high Debye temperature (e.g., Cr, Ni, Ti, Al) could be better choices of metal thermal contacts because of better energy match between phonon modes in these metals and in graphene. Our results enhance the microscopic understanding on heat transport across a single layer of crystalline atoms.

Acknowledgment. This work was supported by DOE Grant DE-FG02-07ER46459, ONR MURI Grant N00014-07-1-0723 (Y.K.K. and D.G.C.), and by ONR Grant N00014-10-1-0061 and the NRI SWAN Center (M.H.B. and E.P.). Sample characterization was carried out in part in the Frederick Seitz Materials Research Laboratory Central Facilities, University of Illinois, which are partially supported by the U.S. Department of Energy under Grants DE-FG02-07ER46453 and DE-FG02-07ER46471.

REFERENCES AND NOTES

(1) Lin, Y.-M.; Dimitrakopoulos, C.; Jenkins, K. A.; Farmer, D. B.; Chiu, H.-Y.; Grill, A.; Avouris, Ph. 100-GHz Transistors from Wafer-Scale Epitaxial Graphene. *Science* **2010**, *327*, 662.

(2) Chen, J.-H.; Chaun, J.; Xiao, S.; Ishigami, M.; Fuhrer, M. S. Intrinsic and Extrinsic Performance Limits of Graphene Devices on SiO_2. *Nat. Nanotechnol.* **2008**, *3*, 206–209.

(3) Balandin, A. A.; Ghosh, S.; Bao, W.; Calizo, I.; Teweldebrhan, D.; Miao, F.; Lau, C. N. Superior Thermal conductivity of Single-Layer Graphene. *Nano Lett.* **2008**, *8*, 902–907.

(4) Seol, J. H.; Jo, I.; Moore, A. L.; Lindsay, L.; Aitken, Z. H.; Pettes, M. T.; Li, X.; Yao, Z.; Huang, R.; Broido, D.; Mongo, N.; Ruoff, R. S.; Shi, L. Two-Dimensional Phonon Transport in Supported Graphene. *Science* **2010**, *328*, 213–216.

(5) Bae, M.-H.; Ong, Z.-Y.; Estrada, D.; Pop, E. Imaging, Simulation, and Electrostatic Control of Power Dissipation in Graphene Devices. *Nano Lett.* **2010**. DOI: 10.1021/nl1011596.

(6) Lee, E. J. H.; Balasubramanian, K.; Weitz, R. T.; Burghard, M.; Kern, K. Contact and Edge Effects in Graphene Devices. *Nat. Nanotechnol.* **2008**, *3*, 486–490.

(7) Ghosh, S.; Calizo, I.; Teweldebrhan, D.; Pokatilov, E. P.; Nika, D. L.; Balandin, A. A.; Bao, W.; Miao, F.; Lau, C. N. Extremely High Thermal Conductivity of Graphene: Prospects for Thermal Management Applications in Nanoelectronic Circuits. *Appl. Phys. Lett.* **2008**, *92*, 151911.

(8) Giovannetti, G.; Khomyakov, P. A.; Brocks, G.; Karpan, V. M. J. van den Brink, and P. J. Kelly, Doping Graphene with Metal Contacts. *Phys. Rev. Lett.* **2008**, *101*, 026803.

(9) Gundrum, B. C.; Cahill, D. G.; Averback, R. S. Thermal Conductance of Metal-Metal Interfaces. *Phys. Rev. B* **2005**, *72*, 245426.

(10) Meric, I.; Han, M. Y.; Young, A. F.; Ozyilmaz, B.; Kim, P.; Shepard, K. L. Current Saturation in Zero-Bandgap, Top-Gated Graphene Field-Effect Transistors. *Nat. Nanotechnol.* **2008**, *3*, 654–659.

(11) Freitag, M.; Steiner, M.; Martin, Y.; Perebeinos, V.; Chen, Z.; Tsang, J. C.; Avouris, P. Energy Dissipation in Graphene Field-Effect Transistors. *Nano Lett.* **2009**, *9*, 1883–1888.

(12) Swartz, E. T.; Pohl, R. O. Thermal Boundary Resistance. *Rev. Mod. Phys.* **1989**, *61*, 605–668.

(13) Lee, S.-M.; Cahill, D. G. Influence of Interface Thermal Conductance on the Apparent Thermal Conductivity of Thin Films. *Microscale Thermophys. Eng.* **1997**, *1*, 47–52.

(14) Koh, Y. K.; Cao, Y.; Cahill, D. G.; Jena, D. Heat-Transport Mechanisms in Superlattices. *Adv. Funct. Mater.* **2009**, *19*, 610–615.

(15) Novoselov, K. S.; Geim, A. K.; Morozov, S. V.; Jiang, D.; Zhang, Y.; Dubonos, S. V.; Grigorieva, I. V.; Firsov, A. A. Electrical Field Effect in Atomically Thin Carbon Films. *Science* **2004**, *306*, 666–669.

(16) Koh, Y. K.; Bae, M.-H.; Cahill, D. G.; Pop, E. Reliably Counting Atomic Planes of Few-Layer Graphene ($n > 4$). Under review.

(17) Ferrari, A. C.; Meyer, J. C.; Scardaci, V.; Casiraghi, C.; Lazzeri, M.; Mauri, F.; Piscanec, S.; Jiang, D.; Novoselov, K. S.; Roth, S.; Geim, A. K. Raman Spectrum of Graphene and Graphene Layers. *Phys. Rev. Lett.* **2006**, *97*, 187401.

(18) Yan, J.; Zhang, Y.; Kim, P.; Pinczuk, A. Electric Field Effect Tuning of Electron-Phonon Coupling in Graphene. *Phys. Rev. Lett.* **2007**, *98*, 166802.

(19) Costescu, R. M.; Wall, M. A.; Cahill, D. G. Thermal Conductance of Epitaxial Interfaces. *Phys. Rev. B* **2003**, *67*, 054302.

(20) Kang, K.; Koh, Y. K.; Chiritescu, C.; Zheng, X.; Cahill, D. G. Two-Tint Pump-Probe Measurements using a Femtosecond Laser Oscillator and Shart-Edged Optical Filters. *Rev. Sci. Instrum.* **2008**, *79*, 114901.

(21) Cahill, D. G. Analysis of Heat Flow in Layered Structures for Time-Domain Thermoreflectance. *Rev. Sci. Instrum.* **2004**, *75*, 5119–5122.

(22) Koh, Y. K.; Cahill, D. G. Frequency Dependence of the Thermal Conductivity of Semiconductor Alloys. *Phys. Rev. B* **2007**, *76*, 075207.

(23) Wang, R. Y.; Segalman, R. A.; Majumdar, A. Room Temperature Thermal Conductance of Alkanedithiol Self-Assembled Monolayers. *Appl. Phys. Lett.* **2006**, *89*, 173113.

(24) Geringer, V.; Liebmann, M.; Echtermeyer, T.; Runte, S.; Schmidt, M.; Rückamp, R.; Lemme, M. C.; Morgenstern, M. Intrinsic and Extrinsic Corrugation of Monolayer Graphene Deposited on SiO_2. *Phys. Rev. Lett.* **2009**, *102*, 076102.

(25) Prasher, R. Graphene Spreads the Heat. *Science* **2010**, *328*, 185–186.

(26) Chen, Z.; Jang, W.; Bao, W.; Lau, C. N.; Dames, C. Thermal Contact Resistance Between Graphene and Silicon Dioxide. *Appl. Phys. Lett.* **2009**, *95*, 161910.

(27) Schmidt, A. J.; Collins, K. C.; Minnich, A. J.; Chen, G. Thermal Conductance and Phonon Transmissivity of Metal-Graphite Interfaces. *J. Appl. Phys.* **2010**, *107*, 104907.

(28) Lui, C. H.; Liu, L.; Mak, K. F.; Flynn, G. W.; Heinz, T. F. Ultraflat Graphene. *Nature* **2009**, *462*, 339–341.

(29) Zheng, X.; Cahill, D. G.; Weaver, R.; Zhao, J.-C. Micron-scale Measurements of the Coefficient of Thermal Expansion by Time-Domain Probe Beam Deflection. *J. Appl. Phys.* **2008**, *104*, 073509.

(30) Persson, A. I.; Koh, Y. K.; Cahill, D. G.; Samuelson, L.; Linke, H. Thermal conductance of InAs Nanowire Composites. *Nano Lett.* **2009**, *9*, 4484.

(31) Pop, E.; Mann, D. A.; Goodson, K. E.; Dai, H. Electrical and Thermal Transport in Metallic Single-Wall Carbon Nanotubes on Insulating Substrates. *J. Appl. Phys.* **2007**, *101*, 093710.

(32) Venugopal, A.; Colombo, L.; Vogel, E. M. Contact Resistance in Few and Multilayer Graphene Devices. *Appl. Phys. Lett.* **2010**, *96*, 013512.

(33) Hu, M.; Keblinski, P.; Schelling, P. K. Kapitza Conductance of Silicon-Amorphous Polyethylene Interfaces by Molecular Dynamics Simulations. *Phys. Rev. B* **2009**, *79*, 104305.

(34) Duda, J. C.; Smoyer, J. L.; Norris, P. M.; Hopkins, P. E. Extension of the Diffuse Mismatch Model for Thermal Boundary Conductance between Isotropic and Anisotropic Materials. *Appl. Phys. Lett.* **2009**, *95*, 031912.

(35) Huxtable, S. T.; Cahill, D. G.; Shenogin, S.; Xue, L.; Ozisik, R.; Barone, P.; Usrey, M.; Strano, M. S.; Siddons, G.; Shim, M.; Keblinski, P. Interfacial Heat Flow in Carbon Nanotube Suspensions. *Nat. Mater.* **2003**, *2*, 731–734.

(36) Wang, Z.; Carter, J. A.; Lagutchev, A.; Koh, Y. K.; Seong, N.-H.; Cahill, D. G.; Dlott, D. D. Ultrafast Flash Thermal Conductance of Molecular Chains. *Science* **2007**, *317*, 787–790.

(37) Cai, W.; Moore, A. L.; Zhu, Y.; Li, X.; Chen, S.; Shi, L.; Ruoff, R. S. Thermal Transport in Suspended and Supported Monolayer Graphene Grown by Chemical Vapor Deposition. *Nano Lett.* **2010**, *10*, 1645.

© 2010 American Chemical Society

DOI: 10.1021/nl101790k | *Nano Lett.* **2010,** *10,* 4363–4368